

# Theoretical development of a high-resolution differential-interference-contrast optic for x-ray microscopy

Olov von Hofsten\*, Michael Bertilson, and Ulrich Vogt

Biomedical and X-ray Physics, Department of Applied Physics, Royal Institute of Technology/Albanova, SE-10691 Stockholm, Sweden

\*Corresponding author: [olov.hofsten@biox.kth.se](mailto:olov.hofsten@biox.kth.se)

**Abstract:** In this paper, the theoretical background and development of a differential-interference contrast (DIC) x-ray optic is presented. The single-element optic is capable of high-resolution phase contrast imaging and is compatible with compact sources. It is shown that an understanding of the coherence requirements in this type of imaging is imperative and is explained in detail. The optic is capable of a wavefront separation equal to the resolution of the optic which places only minor constraints on the object illumination.

©2008 Optical Society of America

**OCIS codes:** (340.0340) X-ray Optics; (180.7460) X-ray microscopy; (050.1970) Diffractive optics.

---

## References and links

1. S. Aoki, Y. Kagoshima, and Y. Suzuki, eds., *X-ray microscopy*, (The Institute of Pure and Applied Physics, Tokyo, Japan 2006).
2. D. T. Attwood, *Soft X-Rays and Extreme Ultraviolet Radiation*, (Cambridge University Press, Cambridge 1999).
3. W. Chao, B. D. Harteneck, J. A. Liddle, E. H. Anderson, and D. T. Attwood, "Soft X-ray microscopy at a spatial resolution better than 15 nm," *Nature* **435**, 1210-1213 (2005).
4. C. A. Larabell and M. A. Le Gros, "X-ray Tomography Generates 3-D Reconstructions of the Yeast, *Saccharomyces cerevisiae*, at 60-nm Resolution," *Mol. Biol. Cell* **15**, 957-962 (2004).
5. G. Schmahl, D. Rudolph, P. Guttman, G. Schneider, J. Thieme, and B. Niemann, "Phase contrast studies of biological specimens with the X-ray microscope at BESSY," *Rev. Sci. Instrum.* **66**, 1282-1286 (1995).
6. G. Schmahl, D. Rudolph, G. Schneider, P. Guttman, and B. Niemann, "Phase contrast X-ray microscopy studies," *Optik* **97**, 181-182 (1994).
7. T. Wilhein, B. Kaulich, and J. Susini, "Two zone plate interference contrast microscopy at 4 keV photon energy," *Opt. Commun.* **193**, 19-26 (2001).
8. T. Wilhein, B. Kaulich, E. Di Fabrizio, F. Romanato, S. Cabrini, and J. Susini, "Differential interference contrast X-ray microscopy with submicron resolution," *Appl. Phys. Lett.* **78**, 2082-2084 (2001).
9. B. Kaulich, T. Wilhein, E. Di Fabrizio, F. Romanato, M. Altissimo, S. Cabrini, B. Fayard, and J. Susini, "Differential interference contrast X-ray microscopy with twin zone plates," *J. Opt. Soc. Am. A* **19**, 797-806 (2002).
10. E. Di Fabrizio, D. Cojoc, S. Cabrini, B. Kaulich, J. Susini, P. Facci, and T. Wilhein, "Diffractive optical elements for differential interference contrast x-ray microscopy," *Opt. Express* **11**, 2278-2288 (2003).
11. U. Vogt, M. Lindblom, P. A. C. Jansson, T. T. Tuohimaa, A. Holmberg, H. M. Hertz, M. Wieland, and T. Wilhein, "Single-optical-element soft-x-ray interferometry with a laser-plasma x-ray source," *Opt. Lett.* **30**, 2167-2169 (2005).
12. C. Chang, A. Sakdinawat, P. Fischer, E. H. Anderson, and D. T. Attwood, "Single-element objective lens for soft x-ray differential interference contrast microscopy," *Optics Letters* **31**, 1564-1566 (2006).
13. P. Fischer, G. Denbeaux, T. Ono, T. Okuno, T. Eimuller, D. Goll, and G. Schutz, "Study of magnetic domains by magnetic soft x-ray transmission microscopy," *J. Phys. D-Appl. Phys.* **35**, 2391-2397 (2002).
14. P. A. C. Takman, H. Stollberg, G. A. Johansson, A. Holmberg, M. Lindblom, and H. M. Hertz, "High-resolution compact x-ray microscopy," *J. Microsc.* **226**, 175-181 (2007).
15. M. Bertilson, O. von Hofsten, and U. Vogt, "Compact high-resolution differential interference contrast soft x-ray microscopy," Submitted to *Appl. Phys. Lett.* (2007).
16. R. D. Allen, G. B. David, and G. Nomarski, "The Zeiss-Nomarski differential interference equipment for transmitted-light microscopy," *Zeitschrift fur Wissenschaftliche Mikroskopie und Mikroskopische Technik* **69**, 193-222 (1969).
17. J. W. Goodman, *Statistical Optics*, (Wiley, New York 1985).

18. C. Preza, D. L. Snyder, and J. Conchello, "Theoretical development and experimental evaluation of imaging models for differential-interference-contrast microscopy," *J. Opt. Soc. Am. A* **16**, 2185-2199 (1999).
  19. O. von Hofsten, P. A. C. Takman, and U. Vogt, "Simulation of partially coherent image formation in a compact soft x-ray microscope," *Ultramicroscopy* **107**, 604-609 (2007).
  20. M. Born and E. Wolf, *Principles of optics: electromagnetic theory of propagation, interference and diffraction of light*, (Cambridge University Press, 1999).
  21. A. G. Michette, *Optical Systems for Soft X Rays*, (Plenum Press, New York 1986).
- 

## 1. Introduction

When phase contrast imaging was first introduced in optical microscopy over 40 years ago, the entire field experienced a leap forward. By utilizing the real part of the complex index of refraction, the contrast in weak absorbing materials such as biological specimens was greatly increased. Since then, two major techniques have become available for phase contrast imaging in optical microscopy, Zernike phase contrast and differential-interference contrast (DIC). DIC is often preferred, since it does not place any limiting requirements on the illumination. In DIC imaging, two mutually coherent wavefronts which are slightly separated are allowed to interfere in the image plane. The two wavefronts are kept mutually coherent since they are separated before the object plane, enabling interference when they are recombined in the image plane.

X-ray microscopy has evolved in the recent years into a successful high-resolution imaging technique [1], where diffractive optics are used as microscope objectives. Such optics are called zone plates and are radial gratings with decreasing grating period. The focal length of such optics is given by [2]

$$f = \frac{4N(\Delta r)^2}{\lambda} \quad (1)$$

where  $N$  is the number of zones and  $\lambda$  is the x-ray wavelength. In addition, it can be shown that the resolution of a transmission x-ray microscope is equal to  $\Delta r$ , the outermost zone width, multiplied by a factor varying between 1.22 and 1.68 depending on the degree of coherent illumination [2]. By recent advances in nanofabrication, resolution down to 15 nm has been proven [3], and tomography of biological specimens is showing great progress [4]. Although the absorption contrast when imaging biological specimens in the so-called water window (2.3 nm – 4.4 nm) is sufficiently high, phase contrast is also interesting, especially when using hard x-rays. X-ray Zernike phase contrast was developed at an early stage [5,6], and is used in a variety of applications, but DIC is still under development. This is mostly due to the difficulties in achieving a sufficiently small wavefront separation and in the fabrication of the necessary optics. The important difference with DIC x-ray imaging from that of optical wavelengths is that the wavefront separation is made by the objective, and the two wavefronts are not recombined as in optical DIC microscopy. Therefore, the mutual coherence of the two wavefronts will also depend on the degree of coherence in the object plane, which in so-called aperture matched conditions decreases to zero in an area corresponding to the resolution of the objective.

We present here the theoretical background to the coherence requirements for x-ray differential-interference-contrast microscopy, and the consequent implementation using a single-element diffractive optic. We will show that an understanding of the illumination conditions is imperative in the design of such an optic. The designed optic provides a wavefront separation equal to the resolution of the optic, placing only small limitations on the illumination. In the future, this can be useful in hard x-ray microscopy where the absorption in biological specimens is low, where instead the phase shift introduced by a specimen will yield sufficient image contrast.

## 2. Experimental work

X-ray interference contrast was first achieved by Wilhein, *et al.*, [7] where two separated zone plates were used to create the wavefronts. Since the mutual separation was much larger than

the resolution of the objective, a high degree of coherence was needed in the object plane. DIC imaging was later accomplished by a twin zone plate with a wavefront separation smaller than 100 nm together with a zone plate with an outermost zone width of 200 nm [8,9]. The small spot separation in combination with the zone plate optic allowed a less coherent illumination, and a condenser optic was used. However, twin zone plates are difficult to fabricate and therefore Di Fabrizio, *et al.*, [10] proposed a single-element optic (diffractive optical element, DOE) using holographic methods to generate the two wavefronts. DIC x-ray imaging was achieved and the method also introduced the concept of bias retardation in x-ray DIC imaging, an important parameter to control the image contrast. Again, a high degree of coherence was used to achieve the DIC effect and only half of the zone plate was used. This was due to the small condenser aperture which caused the +1 and -1 orders of the image to overlap. Holographic methods were also utilized by U. Vogt, *et al.*, [11], although this zone plate was not used in high-resolution DIC x-ray imaging. C. Chang, *et al.*, [12] used a Fourier approach and combined a zone plate lens with a diffraction grating and succeeded with a spot separation of 80 nm. DIC x-ray images of magnetic phase objects were obtained when using an aperture matched condenser and a 40 nm outermost zone width objective. However, since circularly polarized light was needed in this experiment, a large part of the condenser was blocked [13] which increased the coherence in the object plane.

All the examples above were performed at synchrotron sources, where the light economy is more than an order of magnitude better than in compact setups, such as the microscope at BIOX, KTH [14]. In order for an x-ray phase optic to be compatible with compact arrangements, it must permit a more incoherent illumination than in any of the examples above. The optic described in this publication was recently used in successful DIC imaging using the in-house compact soft x-ray microscope [15]. The theoretical spot separation was 50 nm, the outermost zone width of the DOE was 50 nm and the outermost zone width of the condenser was 50 nm. The aim of this publication is to present a theoretical background to these results.

### 3. Theory

#### 3.1 Visible light differential interference contrast microscopy

By comparing x-ray DIC imaging with its visible light counterpart, the necessary requirements can be clarified. Visible light DIC imaging in its current form was first introduced by Nomarski [16] where two modified Wollaston prisms are placed in the optical path. One is placed before the condenser (the so-called compensator) and one is placed slightly beyond the back focal plane of the objective [Fig. 1(a)]. The two mutually coherent images are superimposed and hence the image intensity will depend on the optical path length of the specimen. The resulting image intensity is given by the object phase gradient, which makes the imaging differential. The role of the compensator is to compensate for the phase differences of the light rays emanating from the full width of the condenser. In other words, the compensator ensures full coherence between the two overlapping wavefronts.

There are two important parameters in DIC microscopy, the bias and the shear. The shear is defined as the separation of the two wavefronts, or as a fixed spot separation in the point-spread function (PSF). The bias is a constant phase difference introduced by the upper Wollaston prism and can be varied in order to control the contrast for a given specimen.

#### 3.2 X-ray differential interference contrast microscopy

The optical arrangement in an x-ray DIC microscope is not the same as the equivalent optical microscope [Fig. 1(b)]. The most important difference is that the concept of shear is introduced *after* the object plane. This resembles the early visible light DIC microscopes used without a compensator where instead a slit was placed in front of the condenser, increasing the coherence in the direction of the shear. It is important to realize that the same coherence requirement as in visible light microscopy is necessary in x-ray DIC imaging.

The effect of the DIC optic can be implemented in the image formation process by altering the coherent PSF, creating two separated spots instead of one,

$$k(u, v) = \frac{1}{2} PSF(u + \frac{\Delta u}{2}, v) \exp(i\Delta\theta) + \frac{1}{2} PSF(u - \frac{\Delta u}{2}, v) \exp(-i\Delta\theta) \quad (2)$$

The function  $k(u, v)$  is the coherent field in the image plane created by a point-source in the object plane. The bias and the shear are represented by the two parameters,  $2\Delta\theta$  and  $\Delta u$ , respectively. Equation (2) describes the PSF created by a twin zone plate. In this case, only fabrication issues will limit the desired shear.

When using a single DOE in differential-interference-contrast, the PSF cannot be implemented in this way. Instead, it must be back-calculated from a complex aperture function using the inverse Fourier transform. How shear and bias can be introduced in a DIC-DOE optic is described in section 5 and can be directly observed by investigating the resulting PSF.

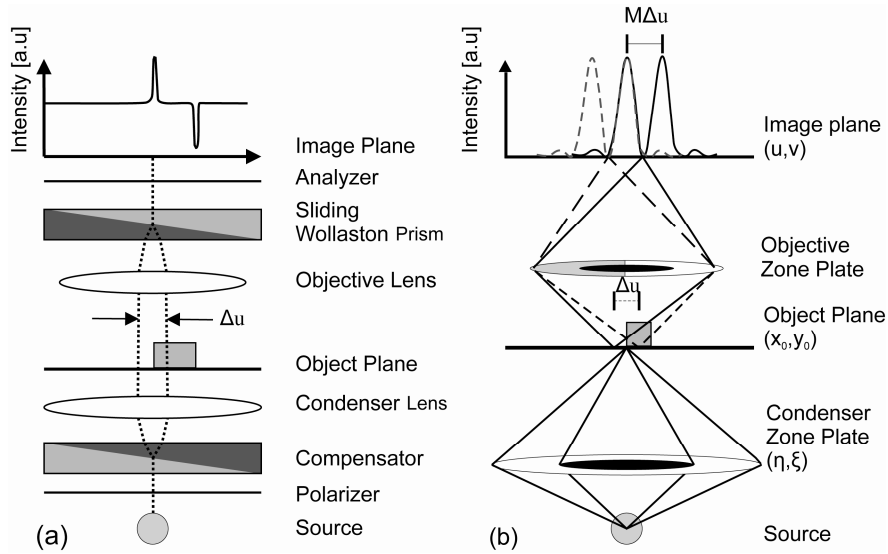


Fig. 1. (a). A Visible light DIC microscope. (b) An x-ray DIC microscope

### 3.3 Coherence requirements for x-ray DIC microscopy

In this section the spatial and temporal coherence requirements for x-ray DIC microscopy will be investigated. In the case of temporal coherence, the requirements are the same as for a normal zone plate, i.e.  $\Delta\lambda/\lambda \leq 1/N$ , where  $N$  is the number of zones and  $\Delta\lambda$  is the bandwidth of the source. For spatial coherence, the requirement can be stated as follows: there must be a sufficient degree of coherence between two points in the object plane separated by the shear produced by the objective DIC zone plate lens. If there is not a sufficient degree of coherence, two points in the object plane separated by the shear will not interfere with each other in the image plane as intended. This statement is illustrated in Fig. 1(b) and a more quantitative description will be provided in the following paragraphs.

The complex degree of spatial coherence in the object plane,  $\mu$ , can be calculated by using the van Cittert-Zernike theorem given by [17],

$$\mu(x_1, y_1; x_2, y_2) = \frac{\kappa e^{-j\psi}}{(\lambda z)^2} \frac{\iint_{\infty} I(\eta, \xi) \exp\left[j \frac{2\pi}{\lambda z} ((x_2 - x_1)\eta + (y_2 - y_1)\xi)\right] d\eta d\xi}{\iint_{\infty} I(\eta, \xi) d\eta d\xi} \quad (3)$$

$I(\eta, \xi)$  is the intensity distribution of the condenser aperture,  $\kappa$  is a constant,  $z$  is the distance between source and object plane and  $\psi$  is a phase factor. All other coordinates are shown in Fig. 1. We will consider the case of uniform, incoherently illuminated and circular apertures, which simplifies Eq. (3) to two Bessel functions of the first order, taking into account that an x-ray condenser optic must have a central stop to separate the 1<sup>st</sup> order rays from the stronger 0<sup>th</sup> order.

To study the effect of coherent illumination in x-ray DIC microscopy, a series of images were calculated. This was carried out using a method based on a model for visible light DIC image formation [18] using partially coherent illumination. Images were calculated using varying shear and degree of coherence, the latter calculated using Eq. (3). The simulation considers the condenser as a secondary source of individually coherent but mutually incoherent emitters, and is described in more detail elsewhere [19]. The image intensity is given by,

$$I_{image}(u, v) = \sum_{n=1}^N \left| k(u, v) \otimes t(u, v) e^{i\varphi(\eta_n, \xi_n)} \right| \quad (4)$$

$t(u, v)$  is the magnified object transmission function which is multiplied by a phase factor,  $\varphi(\eta_n, \xi_n)$  introduced by a point  $(\eta_n, \xi_n)$  on the condenser.  $N$  is the number of point sources used to represent the condenser. By applying Fourier analysis, this expression simplifies to

$$I_{image}(u, v) = \sum_{n=1}^N \left| \mathfrak{F}^{-1} \left\{ \hat{k}(f, g) \hat{t}(f - \Delta f_n, g - \Delta g_n) \right\} \right|^2 \quad (5)$$

In this equation,  $\hat{k}(f, g)$  is the Fourier transform of  $k(u, v)$  and  $\hat{t}(f, g)$  is the Fourier transform of the object transmission function.

Using Eq. (5) together with Eq. (2) and simultaneously calculating a DIC image and an image without DIC, the increase in image contrast could be calculated. In this case, image contrast,  $C$ , is defined in terms of image intensity,  $I$

$$C = \frac{I_{\max} - I_{\min}}{I_{\max} + I_{\min}} \quad (6)$$

In order to separate the phase contrast from absorption contrast, an idealized object was used. It consisted of a 100 % transmitting, 2  $\mu\text{m}$  bar with a phase introduction equal to the introduced bias retardation, both set to  $\pi$ . Due to the infinitely sharp edge and the partially coherent illumination, the image without DIC also shows a certain contrast. The results are plotted in Fig. 2(a), which contains two plots and should provide a quantitative description of the statement in the beginning of section 3.3. The left axis shows the degree of coherence between two points separated by the shear in the object plane plotted in black against the factor  $m$ , a coherence factor defined as the ratio between the numerical aperture of the objective and condenser optic [20],

$$m = \frac{NA_{\text{condenser}}}{NA_{\text{objective}}} \quad (7)$$

The figure shows a plot for two shears, given in terms of the outermost zone width of the objective,  $\Delta r$ . Consistent with theory, the degree of coherence decreases with increasing spot separation and also with increasing coherence factor  $m$ . The right axis shows the increase in image contrast when using DIC instead of a normal optic, plotted in gray against the coherence factor  $m$ . Arrows are displayed to facilitate the interpretation of the figure. Important to notice is that the increase in image contrast decreases with the coherence factor, showing the importance of the illumination conditions in DIC microscopy.

In order to further emphasize the role of the illumination in DIC imaging, Fig. 2(b) shows the edge response for three spot separations and for  $m=0.5$ . Again, the smallest spot separation yields the highest contrast in the image.

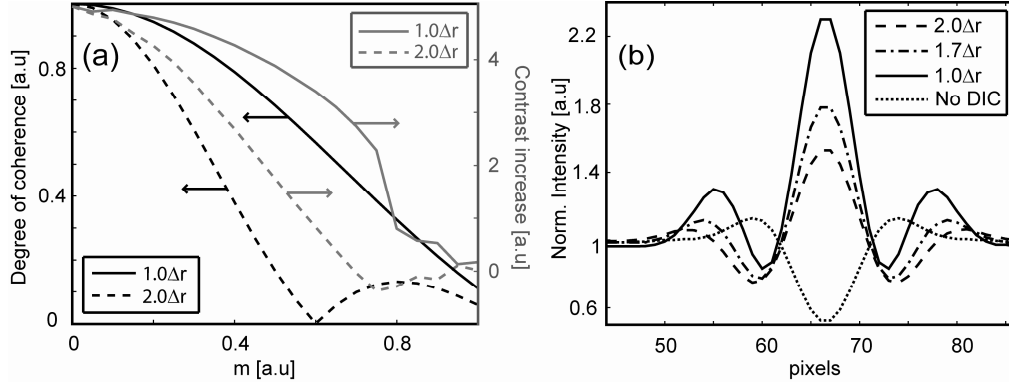


Fig. 2. (a). The degree of coherence (left axis, in black) and the contrast increase (right axis, in gray) versus the coherence factor  $m$  for two shears. The arrows point to the appropriate y-axis. (b). Edge response for  $m=0.5$  for three different shears and without DIC. The bias retardation and the phase of the object were both set to  $\pi$  and there was no absorption in the object.

#### 4. Realization of the single element differential-interference-contrast objective

The results in the previous section indicate that two conditions must be fulfilled in order to achieve successful DIC imaging: a shear close to the resolution of the optic and a partially coherent illumination. A higher degree of coherence will yield a larger contrast increase, but at the same time place limitations on the illumination. We will now continue to show how the two requirements can be fulfilled by using a single optical element, or a DIC-DOE.

In order to find the design of a DOE yielding the PSF given in Eq. (2), we will first find a complex aperture function and then calculate its corresponding zone plate pattern. This method can be applied to any of the DOEs outlined in section 2 and is valid if the DOE has more than 100 zones [21]. Consequently, any phase-shift in the complex aperture function will correspond to a shifting of the zones in the DOE. The complex aperture function for the DIC PSF given in Eq. (2) is given by

$$A(f, g) = \mathfrak{F}^{-1}(k(u, v)) = (2\pi)^2 \hat{k}(-f, -g) \quad (8)$$

Where  $\mathfrak{F}^{-1}$  represents the inverse Fourier transform. The Fourier transform of Eq. (2),  $\hat{k}(f, g)$ , can be carried out analytically.  $A(f, g)$  is thus given by

$$A(f, g) = (2\pi)^2 \cos\left(\Delta\theta - 2\pi f \frac{\Delta u}{2}\right) P\hat{S}F(f, g) \quad (9)$$

When this function corresponds to the DOE in phase and magnitude, it will yield the same shear and bias as  $k(u, v)$ . Since  $A(f, g)$  is a real function, the phase is either 0 or  $\pi$  and the frequency where the change takes place is given by,

$$f_{cut} = \frac{2\Delta\theta + l\pi}{2\pi\Delta u} \quad (10)$$

where  $l=\pm 1, \pm 2$ , and so on. A phase shift of  $\pi$  corresponds to moving the zones one half period or in other words, inverting the pattern of the DOE where the phase-shift takes place. This means that there is a corresponding position on the zone plate where the phase-shift (called

phase cut from now on) will take place. The frequency  $f_{cut}$  corresponds to a distance,  $d_{cut}$ , from the center of the zone plate in the shear direction which can be normalized to the radius of the optic,  $r$

$$\frac{d_{cut}}{r} = \frac{\Delta r(2\Delta\theta + l\pi)}{\pi\Delta u} \quad (11)$$

As seen, the position for the phase cut depends on both the shear and the bias. By applying Eq. (11) to the case of two phase cuts, giving a defined grating constant, the shear and the bias can be calculated in the same way as given in ref. [12]. However, if  $\Delta r = \Delta u$ , there can be only one cut in the optic. But if there is only one phase cut in the optic, Eq. (11) has an infinite number of solutions. To fully determine the bias and shear, one must study the magnitude of the complex aperture function, which will contain enough information about the grating period to completely determine the bias and shear. Unfortunately, this would require a zone plate with a varying absorption which, putting aside the obvious fabrication difficulties, is not feasible since the efficiency of a zone plate is also dependent on its thickness. This means that the magnitude of the complex aperture function is simply set to one for the DOE pattern, and therefore Eq. (11) has an infinite number of solutions. However, one can calculate the PSF from a zone plate pattern where a single phase cut is placed at varying positions and measure the shear and bias directly. The relation is illustrated in Fig. 3. which shows a plot of bias and shear as a function of the position of the single phase cut, in terms of the radius of the zone plate. By placing the phase cut at half the radius, a shear of  $\Delta r$  is achieved together with a bias of  $\pi/3$ . The first of the two requirements are thus fulfilled, namely a shear equal to the resolution of the optic.

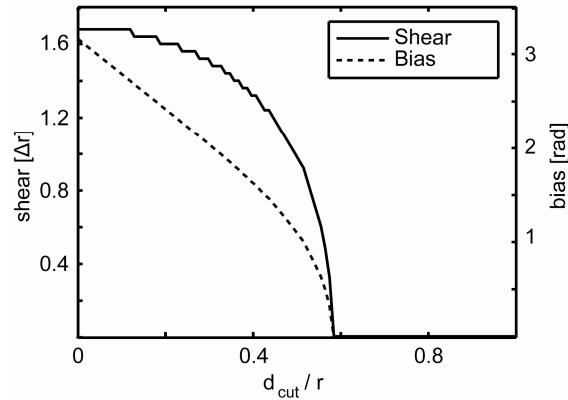


Fig. 3. Bias and shear (expressed in terms of the outermost zone width) measured in the 2D PSF as a function of the position of the phase cut. As seen, the position of the phase cut affects both the shear and the bias.

Given this information, a zone plate was designed where the pattern was phase-shifted by  $\pi$  in one direction at a distance larger than half the radius. In practice, this means that the phase-shifted zone plate pattern is reversed [see Fig. 4(b)]. The resulting one-dimensional PSF was calculated using wave-propagating methods and is compared to the PSF from a complex aperture function and to that of a normal zone plate in Fig. 4(a). The aperture function is defined as one on the zone plate optic and zero outside, but also has a phase cut as described earlier. The two DIC PSFs are consistent apart from a small asymmetry in the PSF calculated from the DOE pattern. The effect of this asymmetry has not been investigated, but it is not likely that it will cause any major differences between images simulated using a DOE pattern or the corresponding complex aperture function. Therefore, it is reasonable to use the complex aperture function instead of the DOE pattern when simulating images. Fig. 4(b) shows the pattern of the designed DIC-DOE optic, from now on referred to as the side-cut DOE. The

results confirm that by positioning the phase cut at half the radius, a shear of  $\Delta r$  is achieved. The necessary degree of coherence can be found from Fig. 1(a). For the given shear, an  $m$  value smaller than 0.6 will yield a contrast increase of 3 times or more.

As seen in Fig. 3 the shear can be made smaller by placing the phase cut farther to the side which would relax the conditions on the coherent illumination. However, Fig. 3 also shows that this will yield a smaller bias, which reduces the contrast in the image.

Given the benefits of a single-component DIC optic, there are a few drawbacks. First off, a DIC x-ray microscope does not have the possibility of changing bias without changing optic. This limits the possibility of controlling the contrast for a given specimen. In addition, the limitation in spot separation of  $\Delta r$  will require partially coherent illumination, limiting the possible size of the condenser. However, this is also a problem for Zernike phase contrast methods.

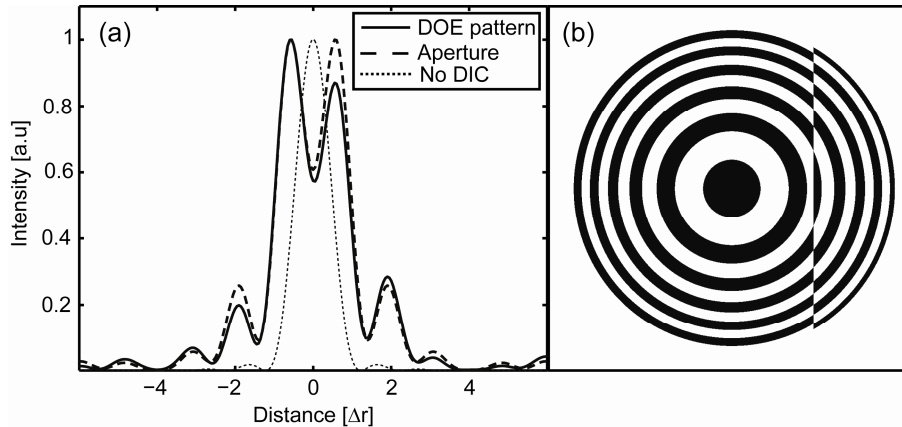


Fig. 4. (a). The calculated one-dimensional PSF from a DOE pattern (solid) compared with the PSF from the corresponding complex aperture function (dashed). The PSF calculated from the aperture of a conventional zone plate is also shown. (b) The resulting side-cut DOE.

## 5. Results from simulations

Images of Siemens stars were simulated with different shear and bias. As explained earlier, this was implemented by moving the phase-cut in the aperture function. The results are shown in Fig. 5. and confirm that the coherence in the object plane together with the shear fully determines the DIC effect. The figure shows three images together with their corresponding zone plates simulated with equally coherent illumination. Two images were simulated with a shear in the PSF and for comparison an image formed by a normal zone plate is also shown. The parameters were set to simulate the situation of the compact soft x-ray microscope at BIOX, KTH [14]. Therefore, the condenser and objective have a numerical aperture of  $NA_{CZP}=0.0126$  and  $NA_{OZP}=0.025$  respectively. This yields a coherence factor of  $m=0.5$ . The outermost zone of the objective was 50 nm and the illuminating wavelength was set to 2.48 nm. In Fig. 5(a), an image simulated with the side-cut DOE optic is shown. An image formed with a zone plate with a phase cut in the center (XOR pattern) is shown in Fig. 5(b). This corresponds to a shear of about 80 nm. To differentiate between absorption and phase contrast, the object was completely transparent, which is a good approximation when imaging biological samples with hard x-rays. In addition, the object introduced a phase shift equal to the bias of the side-cut DOE, which was previously calculated to  $\pi/3$ . The three images show that the side-cut DOE objective yields the best contrast, especially for high frequencies. The characteristic dark and bright outlines of the spokes are clearly seen, as expected in DIC imaging with this type of bias.

To further emphasize this conclusion, intensity line plots of the images are shown in Fig. 6(a). A profile of the object phase is also included, showing the edge response of the different optics. The line plot taken from the XOR zone plate image shows no increase in modulation

compared to the normal zone plate image. However, the side-cut DOE image shows an increase in modulation by a factor of three, which is in agreement with the plot in Fig. 2(a).

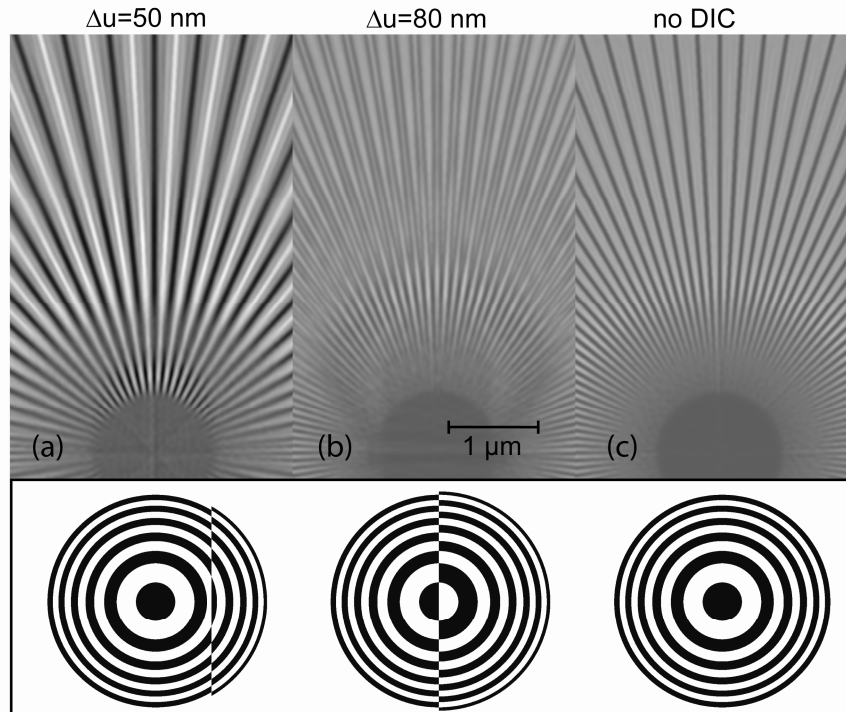


Fig. 5. (a, b). Simulated images using DIC zone plates and (c). using a conventional zone plate. The lower images show the corresponding zone plates. The image simulated using a side-cut DOE, (a), exhibits the best contrast.

In addition to the contrast increase seen in Fig. 5(a), the resolution in the image is not decreased when compared to the image formed by a normal zone plate seen in Fig. 5(c). In fact, the resolution seems to have increased when using the side-cut DOE. However, this is due to the phase object imaged with the normal zone plate. If the simulation is carried out with absorption in the object, it can be seen that the resolution with the normal zone plate and the side-cut DOE is the same. This is due to that the shear is equal to the resolution of the objective, which is why the same high-resolution is not seen in the Fig. 5(b), where a shear larger than the resolution is used. Note that this is consistent with the comparisons between the PSFs shown in Fig. 4. The DIC PSF is broader than that of a normal zone plate but since the phase varies over the shear, the resolution is not limited by the width of the PSF but by the shear of the optic.

An interesting observation from the DIC image in Fig. 5(a) is that the image contrast is not decreasing with smaller grating period. Instead, it takes on a more cyclic dependence. This is likely due to the binary pattern of the zone plate which cannot include the magnitude of the complex aperture function, as described in section 4. The effect is not seen with a twin zone plate, and neither for a DIC zone plate with more than one phase cut.

The image contrast when using a DIC optic will, besides the factors already discussed, depend on the bias of the optic and the phase shift introduced by the object. To show how the phase shift of the object affects the performance of the DOE, Fig. 6(b) shows a plot of image contrast versus the phase shift of the object. The side-cut DOE yields the best contrast when the phase shift of the object is smaller than  $2\pi/3$ . The simulation also indicates that for larger

phase shifts, a normal zone plate will yield the best contrast when imaging a completely transparent object and using the given illumination setup.

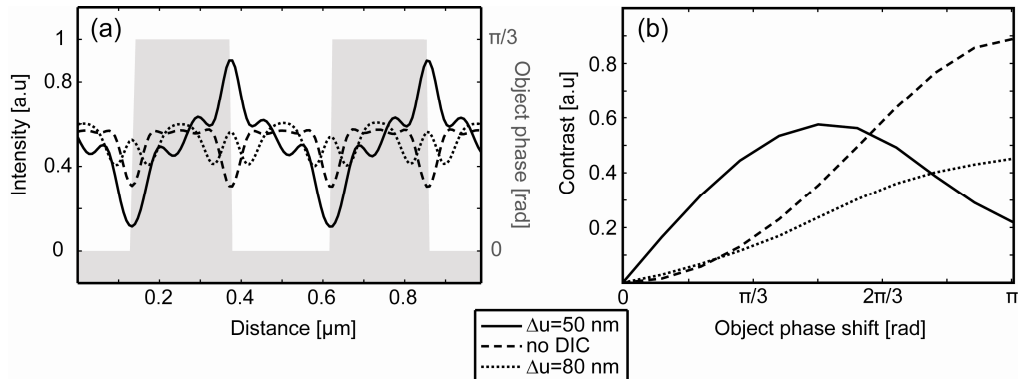


Fig. 6. (a). Intensity profiles of the images shown in Fig. 5. The image taken with the side-cut DIC optic where the shear is 50 nm shows the best contrast. Also shown is the phase of the object, varying between zero and  $\pi/3$ . (b) Image contrast for the same spatial frequency as in (a) but for different object phase shifts. The side-cut DOE objective yields the best contrast for objects where the phase shift is smaller than  $2\pi/3$ .

## 6. Conclusions

We have investigated the coherence requirements for single-element DIC imaging in x-ray microscopy and described the development of a side-cut DOE, capable of a shear equal to the resolution of the optic. Successful DIC imaging can be accomplished if there is enough degree of coherence between two points in the object plane separated by the shear. The shear is defined by the position of the phase cut in the optic and the degree of coherence can be adjusted by the numerical aperture of the condenser. A suitable configuration when the shear is equal to the resolution of the optic was found to be an  $m$ -value of 0.5. The shear is provided when the phase cut is positioned at a distance of half the radius from the center of the optic. The shear can be made smaller by moving the phase cut of the object further to the side but simulations showed that this was not beneficial for optimal phase contrast imaging. Simulated images showed a modulation increase by a factor of three, proving that the designed optic can be used in phase contrast x-ray microscopy. In addition, there is no decrease in resolution compared to a normal zone plate. The side-cut DOE objective has been successfully tested in the in-house compact soft x-ray microscope [15] where a contrast increase of a factor of two was found compared to a conventional zone plate. The quantitative difference between the experiment and the simulation can be explained by the object imaged by the soft x-ray microscope, which also exhibited absorption. The results suggest further experiments in the hard x-ray regime.

## Acknowledgments

The authors would like to thank Kjell Carlsson and Hans Hertz for important discussions leading up to this work. This project has been funded by the Swedish Research Council.